JOURNAL OF PHYSICAL ORGANIC CHEMISTRY, VOL. 11, 546–560 (1998)

Review Commentary

Gated molecular and biomolecular optoelectronic systems via photoisomerizable monolayer electrodes†

Itamar Willner,* Amihood Doron and Eugenii Katz

Institute of Chemistry and Farkas Center for Light-Induced Processes, The Hebrew University of Jerusalem, Jerusalem 91904, Israel

Received 21 July 1997; revised 18 January 1998; accepted 4 February 1998

ABSTRACT: Molecular and biomolecular optobioelectronic systems that yield the amperometric transduction of recorded optical signals are described. Phenoxynaphthacene quinone is assembled as a monolayer on an Au electrode. Photoisomerization of the monolayer between the redox-active *trans*-quinone state and the redox-inactive 'ana'-quinone state provides a means to transduce electrochemically optical signals recorded by the monolayer. Coupling of the redox-active *trans*-quinone monolayer electrode to the secondary reduction of *N*,*N*′-dibenzyl-4,4′-bipyridinium, BV^{2+}, provides a means to amplify the transduced current. As the redox potential of the *trans*-quinone monolayer is pH dependent, the electrocatalyzed monolayer-mediated reduction of BV^{2+} is controlled by light and the pH. The system represents an 'AND' gated molecular electronic assembly. A thiol nitrospiropyran monolayer was assembled on an Au electrode. The functionalized electrode acts as photo-triggered 'command interface' that controls the electrooxidation of dihydroxyphenylacetic acid (DPAA). The electrical properties of the monolayer are controlled by the photoisomer state of the monolayer and the pH of the medium. The monolayer in the nitromerocyanine state exists at pH 9.2 and 7.0 in zwitterionic or positively charged states, respectively. Electrooxidation of the negatively charged substrate, DPPA, is enhanced only in the presence of the protonated nitromerocyanine monolayer electrode. This permits the gated oxidation of the substrate by two complementary triggering signals, light and pH. A mixed monolayer consisting of nitrospiropyran and thiolpyridine units assembled on an Au electrode is applied as a photoisomerizable command surface for controlling the electrical contact of cytochrome *c* (Cyt *c*) with the electrode. In the nitrospiropyran–pyridine configuration electrical contact of Cyt *c* and the electrode is attained by the association of Cyt *c* to pyridine promoter sites. Photoisomerization of the monolayer to the protonated nitromerocyanine state results in the electrostatic repulsion of Cyt *c* from the monolayer, and the electrical contact of Cyt *c* with the electrode is blocked. Coupling of the electrically contacted Cyt *c* and nitrospiropyran–pyridine monolayer electrode configuration to the cytochrome oxidase biocatalyzed reduction of oxygen provides a means to amplify the transduced amperometric response. The photostimulated association and dissociation of Cyt *c* to and from the photoisomerizable monolayer were confirmed by microgravimetric, quartz crystal microbalance analyses. The system mimics the function of the native vision process.

KEYWORDS: molecular optoelectronics; bio-optoelectronics; photoisomerizable monolayers; functionalized electrodes; photoactive monolayers; photochemical switch; optical switches; molecular electronic gates; cytochrome *c*; cytochrome oxidase; protein monolayer interactions; quartz crystal microbalance; photochromic compounds; redox switch

INTRODUCTION

Triggering of chemical functions by external signals and subsequent physical transduction of the activated chemical functionality represent the basic features of intelligent chemical assemblies (ICA). ICA provide basic elements to design sensory systems, information storage devices, molecular electronic systems, molecular machinery and other signal-triggered/response chemical assemblies.[1–9] To tailor ICA, the organization of molecular systems which are triggered by external signals such as optical, electrical, thermal, magnetic or pH, to a chemical function, is essential. The transduction of the activated chemical functionality can proceed by electronic, optical, chemical or spectroscopic outputs. Several basic features characterize ICA:

(i) Activation and deactivation of the ICA should proceed in a cyclic, signal-controlled manner. No component of the ICA should be depleted upon operation.

†Presented at the 6th European Symposium on Organic Reactivity.

**Correspondence to:* I. Willner, Institute of Chemistry and Farkas Center for Light-Induced Processes, The Hebrew University of Jerusalem, Jerusalem 91904, Israel.

Contract/grant sponsor: Israel Science Foundation.

 CCC 0894–3230/98/080546–15 $17.50

(ii) The response time of the signal sensory unit and the transducing system should be rapid and reveal a high signal-to-noise ratio.
(iii) Amplified transduction of the recorded signal and the activated chemical functionality is advantageous to yield sensitive ICA. This allows the activation of the chemical assemblies with weak input signals, and the amplification of recorded information.
(iv) In various ICA, the capability for storage of the recorded activating signal and the subsequent retrieval and transduction of the stored information at any time is requested. The read-out of the stored information followed by the erasure of the stored data yield ICA of write–store–read–erase capabilities.
(v) Integration of the chemical sensory and transduction elements of the ICA on a surface is expected to yield solid-state devices at the molecular level.

Scheme 1 outlines schematically the operation of an optoelectronic switch, a simple ICA. A molecular component, A, is assembled on an electrode support. In this state, the molecular function is redox-inactive and the system is electrically mute. Photoisomerization of A to the molecular state B yields a redox-active molecular interface, and the functionalized electrode transduces amperometrically the recorded optical signal. Under conditions where the photoisomerized state B is thermally stable, the recorded optical signal can be read out electrically at any time. Provided that the functionalized interface in state B stimulates the electrocatalyzed reduction (or oxidation) of a substrate (S) to a product (P), the initial optical activation signal is transduced as an amplified electronic output due to the electrocatalytic transformation. If the photosensitive functionalized monolayer exhibits reversible photoisomerizable properties, the back photoisomerization of state B to A regenerates the mute, redox-inactive, interface. Hence, the system represents an ICA of write–store–read–erase capabilities.

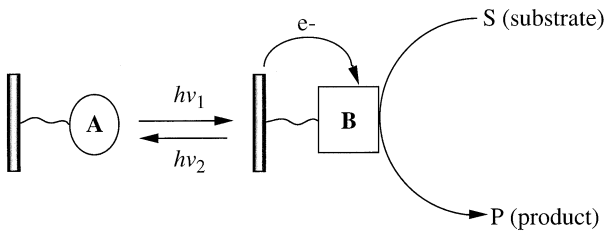

Scheme 1. Monolayer assembled system providing an optical switch between electrochemically inactive (A) and electrochemically active (B) components. Component B storing the information and existing in two redox states (reduced and oxidized) can be used to read the information amperometrically and lock the information by applying a certain potential. The amperometric response can be amplified by electrocatalytic reaction

Photoisomerizable chemical systems that alter their redox properties as a function of the photoisomer state allow the amperometric transduction of recorded optical signals.[10–14] Integration of redox-activated photoisomerizable compounds with electrode supports provides a means for tailoring organized molecular assemblies for the electronic transduction of recorded optical signals. For example, the different redox features of *trans*- and *cis*-azobenzene were used to organize photoisomerizable azobenzene monolayers on conductive supports for the amperometric transduction of optical information recorded by the monolayer interface.[15,16] A different approach to organizing molecular optoelectronic systems includes the functionalization of electrodes with molecular components that control the association or dissociation of photoisomerizable redox-active components with the monolayer interface.[17–19] For example, the functionalization of Au electrodes with a xanthene dye π-donor monolayer[17,18] or with a β-cyclodextrin receptor monolayer[19] permitted the photostimulated formation or dissociation of supramolecular donor–acceptor complexes or host–guest complexes between photoisomerizable substrates and the respective monolayer interfaces.

Photostimulation of biomolecular systems provides a means to organize optobioelectronic systems.[20] The design of integrated photoswitchable systems based on redox-activated enzymes allows the electronic amplification of photonic signals recorded by the biomaterial via the bioelectrocatalyzed oxidation (or reduction) of the enzyme substrate. Various methods to photostimulate the bioelectrocatalytic properties of redox enzymes have been applied to organize optobioelectronic systems. Chemical modification of redox enzymes, e.g. glucose oxidase, with photoisomerizable units and immobilization of the photoisomerizable biocatalysts as monolayers on electrodes yielded photoswitchable enzyme electrodes for the amperometric transduction of photonic signals.[21] Reconstitution of a flavoenzyme, e.g. glucose oxidase with a photoisomerizable FAD cofactor, led to a photoswitchable semi-synthetic enzyme.[22] Assembly of the reconstituted biocatalyst on an electrode generated an active bio-interface for the amplified electrochemical transduction of optical signals that trigger the enzyme monolayer. Photoisomerizable monolayers assembled on electrode supports were used as 'command interfaces' that control the electrical contact of redox enzymes with the electrode surface.[23] In these systems, the photonic signals trigger the physicochemical properties of the monolayer, and these control the interactions of redox enzymes and the resulting electrical contact between the biocatalysts and the electrode. A further means to photostimulate the bioelectrocatalytic properties of redox enzymes includes the application of photoisomerizable electron mediators for electrical contacting of the biocatalyst redox center and the electrode.[24]

This paper addresses recent developments in the organization of molecular and biomolecular ICA. Several

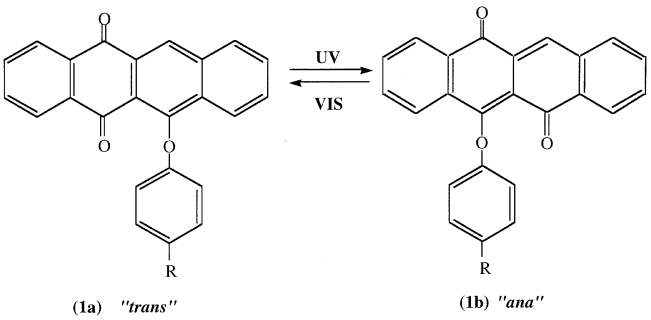

(1a) *"trans"* (1b) *"ana"*

Scheme 2. Photoisomerizable phenoxynaphthacenequinone derivatives

systems that accomplish the electrochemical transduction of optical signals triggering chemical functionalities are described. The relation of optically stimulated chemical assemblies to solid-state electronic devices is emphasized.

A PHENOXYNAPHTHACENE QUINONE MONOLAYER ASSEMBLED ON A GOLD ELECTRODE: A MOLECULAR OPTOELECTRONIC SYSTEM[25]

Phenoxynaphthacene quinone (**1a**) exhibits reversible photoisomerizable properties. Irradiation of **1a** between 305 and 320 nm, yields the rearranged 'ana'-quinone derivative, **1b**. Further irradiation of **1b** with visible light above 430 nm, regenerates the quinone substrate **1a** (Scheme 2). The trans-quinone, **1a** and the 'ana'-quinone, **1b** are expected to exhibit different redox features and thus optical signals recorded by this molecular system could be transmitted electrochemically. Nevertheless, neither **1a** nor **1b** reveals defined diffusional redox responses. This limitation is resolved, however, by chemical functionalization of an Au electrode with the phenoxynaphthacene quinone substrate. The quinone-functionalized electrode yields an integrated molecular electronic system for the cyclic amperometric transduction of recorded optical signals. Scheme 3 shows the method to assemble the quinone on the Au support. A primary cystamine monolayer was assembled on the electrode and 4-carboxymethyl phenoxynaphthancene quinone (**2a**) was coupled to the monolayer interface using 1-ethyl-3-(3-dimethylaminopropyl)carbodiimide (EDC) as coupling reagent. Figure 1, curve a, shows the cyclic voltammogram of the resulting monolayer electrode. The electrical response is irreversible and ill-defined. This is consistent with other observations of irreversible electrical responses of non-densely packed π-conjugated systems and particularly quinone monolayers. Presumably, the non-densely packed π-conjugated quinone interacts with the electrode surface, yielding different orientations of the redox-active quinone relative to the surface. The different quinone orientations result in different interfacial electron transfer rate constants and a

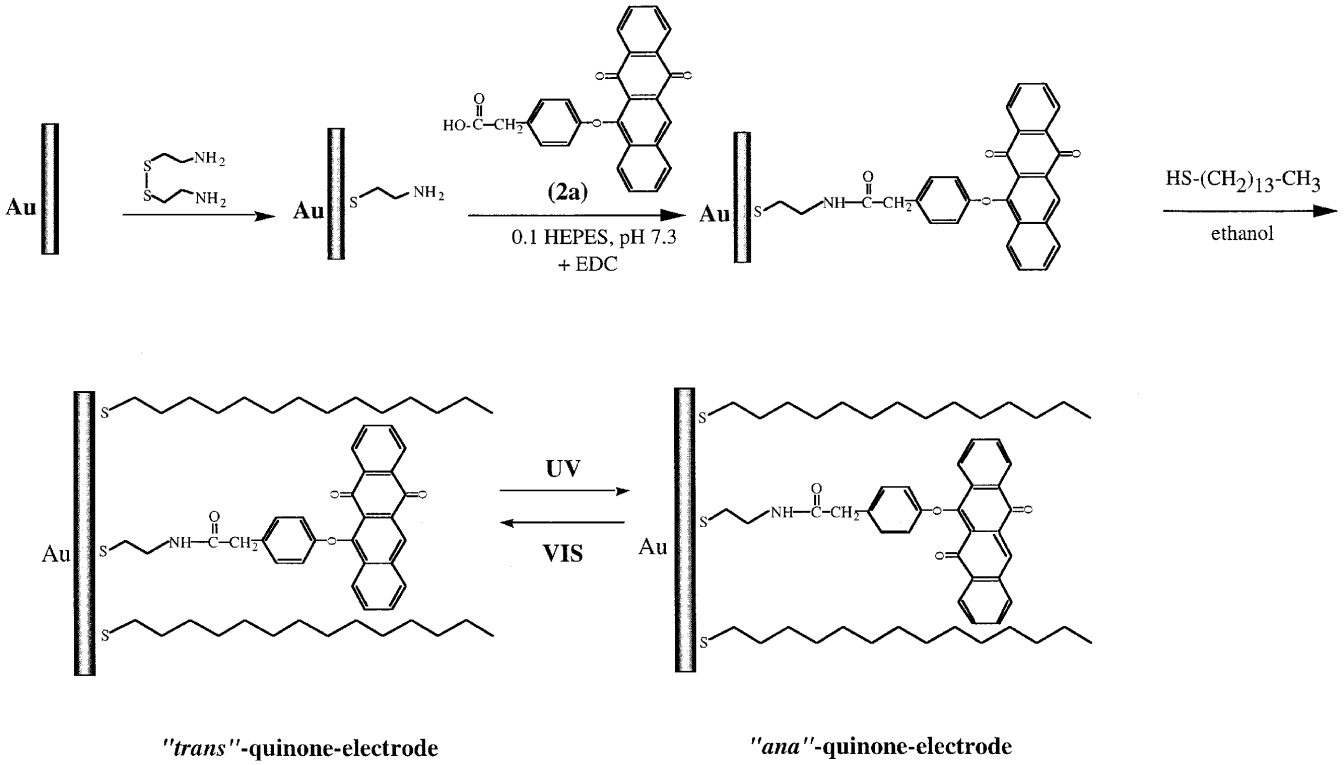

"trans"-quinone-electrode *"ana"*-quinone-electrode

Scheme 3. Assembly of the phenoxynaphthacenequinone–$C_{14}SH$ mixed monolayer on an Au electrode and its photoisomerization

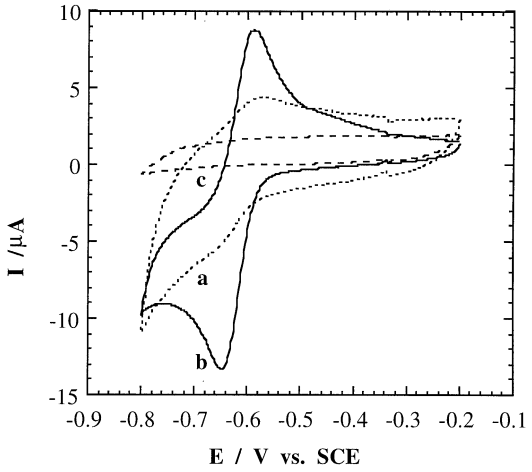

Figure 1. Cyclic voltammograms of (a) **2a** monolayer-modified Au electrode, (b) **2a** monolayer-modified Au electrode after treatment with an ethanolic solution of $C_{14}H_{29}SH$ (5×10^{-3} M) for 30 min, and (c) **2b** monolayer-modified Au electrode obtained by photoisomerization of the **2a** monolayer-modified Au electrode treated with $C_{14}H_{29}SH$ (305–320 nm). All experiments were performed in 0.01 M phosphate buffer and 0.1 M Na_2SO_4 (pH 7.0); potential scan rate, 50 mV s^{-1}

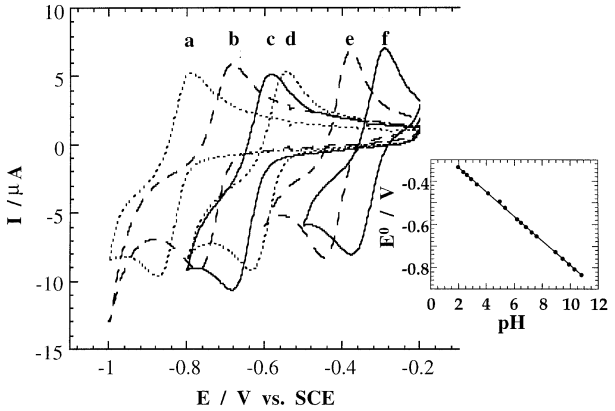

Figure 2. Cyclic voltammograms of the **2a**–$C_{14}SH$ mixed monolayer Au electrode at different pH values: (a) 10.82, (b) 8.93, (c) 7.27, (d) 6.48, (e) 3.32 and (f) 1.93. Background, 0.05 M Britton–Robinson buffer titrated to the required pH value directly in the cell; potential scan rate, 50 mV s^{-1}. Inset: E° vs pH dependence

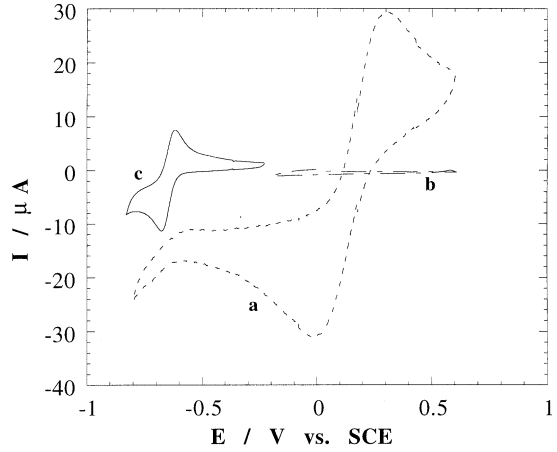

Figure 3. Cyclic voltammograms of (a) $K_3[Fe(CN)_6]$ (1×10^{-3} M) at a bare Au electrode, (b) $K_3[Fe(CN)_6]$ (1×10^{-3} M) at a **2a**–$C_{14}SH$ mixed monolayer Au electrode and (c) a **2a**–$C_{14}SH$ mixed monolayer Au electrode in the absence of $K_3[Fe(CN)_6]$. Background, 0.01 M phosphate buffer and 0.1 M Na_2SO_4 (pH 7.5); potential scan rate, 50 mV s^{-1}

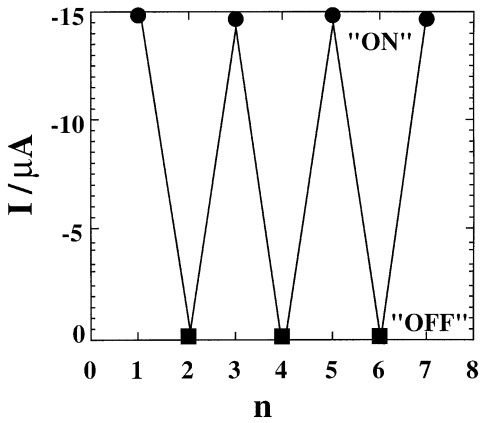

Figure 4. Cyclic variations of peak currents of the **2a**–**2b**–$C_{14}SH$ mixed monolayer Au electrode upon reversible transformation of the quinone from the *trans*-state (**2a**) to the 'ana'-state (**2b**), respectively. Peak currents are derived by subtraction of the capacitive current from the observed peak currents

poorly defined redox response of the monolayer. Treatment of the quinone-functionalized electrode with tetradecylthiol ($C_{14}SH$) results in the electrical response shown in Fig. 1, curve (b). A quasi-reversible redox wave of the quinone units, $E^{\circ} = -0.62$ V vs SCE at pH 7.0, is observed. Figure 2 shows the changes in the quinone redox potential at various pH values. A linear relationship (slope = 56.2 mV pH^{-1}; Fig. 2, inset) is observed within the pH range 2.0–10.5, implying that the redox process of the phenoxynaphthacene quinone monolayer corresponds to a two-electron and two-proton transformation producing the corresponding hydroquinone. Coulometric analysis of the reduction (or oxidation) wave of the quinone monolayer indicates a surface coverage of 2×10^{-10} mol cm^{-2} of the redox-active component.

The transformation of an ill-defined redox response of an Au surface-confined redox species to quasi-reversible electrochemical behavior upon treatment with a long-chain, hydrophobic, alkanethiol has been established before. Long-chain thiols self-assemble on Au surfaces and yield densely packed two-dimensional arrays. As the phenoxynaphthacene quinone monolayer exists in a non-dense configuration, the alkanethiols associate with the Au surface defects or pinholes. The co-associated alkanethiol turns the monolayer into a densely packed array, and the quinone units are stretched into a rigidified structure that reveals quasi-reversible redox features. The

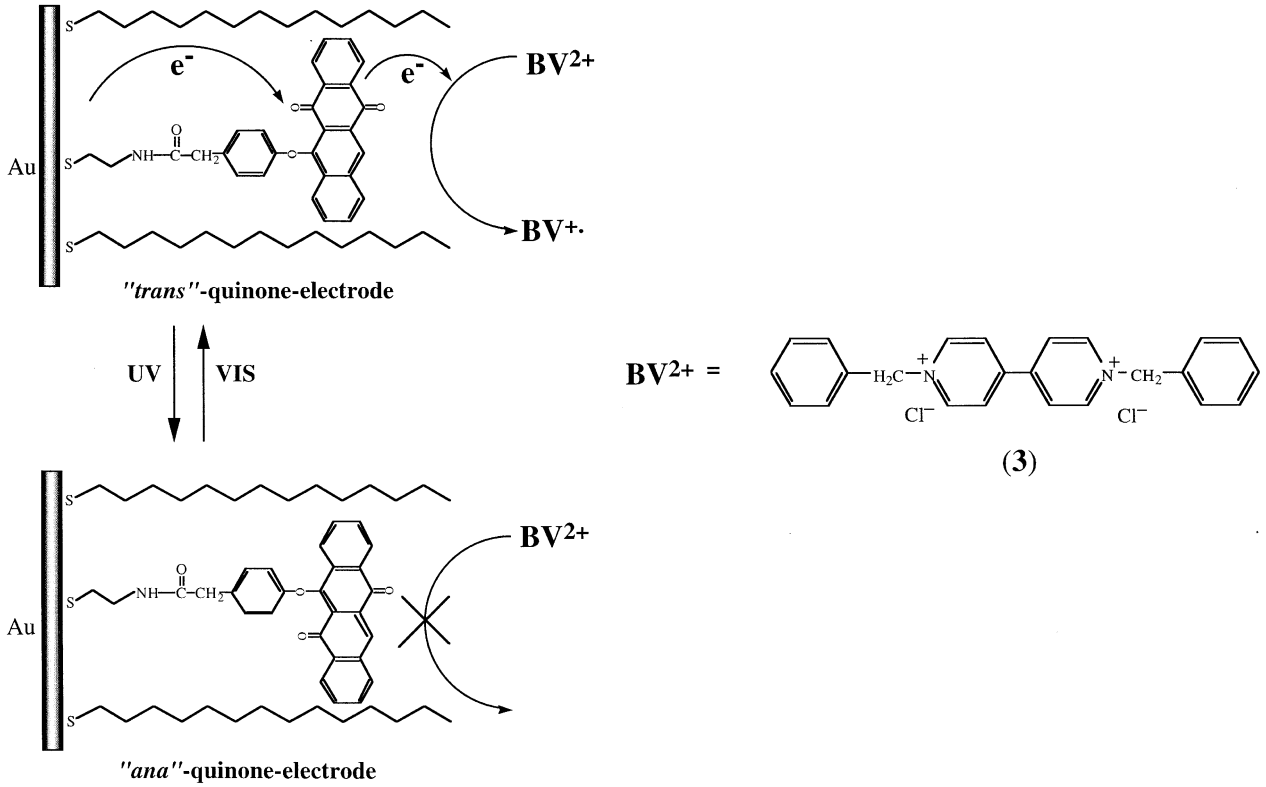

Scheme 4. Photoswitchable electrocatalytic reduction of N,N′-dibenzyl-4,4′-bipyridinium salt, BV^{2+} **(3),** at the phenoxynaphthacene quinone–C_{14}SH mixed monolayer electrode interface

peak current of the phenoxynaphthacene quinone redox wave is directly proportional to the scan rate (v), consistent with the behavior of a surface-confined redox component. The densely packed nature of the alkanethiol–quinone-functionalized monolayer is supported by the fact that the electrode support is insulated towards interfacial electron transfer. Figure 3 shows the cyclic voltammogram of an $Fe(CN)_6^{3-}$ electrolyte solution at a bare Au electrode, curve a, and at the alkanethiol–quinone monolayer electrode, curve b. While $Fe(CN)_6^{3-}$ exhibits a reversible redox wave at the bare electrode, its reduction is entirely blocked at the quinone–alkanethiol mixed-monolayer-functionalized electrode. The electrical contact between the solubilized redox species and the electrode is blocked by the non-conductive, densely packed, hydrophobic monolayer associated with the electrode. Note that in the system, the redox response of $Fe(CN)_6^{3-}$ is examined in a potential window at which the monolayer is electrochemically inactive. The cyclic voltammogram of the **2a**–C_{18}SH monolayer-modified electrode in the absence of $Fe(CN)_6^{3-}$ is shown in Fig. 3, curve c. Expansion of the potential window (curve a at potentials <-0.6 V) could facilitate electrocatalyzed reduction (or oxidation) of solution solubilized redox species (see below).

Photoisomerization of the alkanethiol–phenoxynaphthacene quinone monolayer between 305 and 320 nm results in an electrode with the electrical response shown in Fig. 1, curve c. The redox wave characterizing the electrode is depleted and only the background current of the electrolyte solution is observed. Hence the 'ana'-quinone monolayer is redox-inactive within this potential range. Further irradiation of the 'ana'-quinone monolayer above 430 nm regenerates the phenoxynaphthacene quinone monolayer, and its characteristic redox response is reactivated. By cyclic photoisomerization of the monolayer between the quinone and 'ana' states, the electrical responses of the functionalized electrode are switched on and off, respectively (Fig. 4). Hence the phenoxynaphthacene quinone monolayer electrode acts as an active interface for the amperometric transduction of optical signals recorded by the functionalized conductive support.

ELECTRICAL AMPLIFICATION AND DESIGN OF A MOLECULAR 'AND' GATE BY THE PHENOXYNAPHTHACENE QUINONE MONOLAYER ELECTRODE

The system exhibits several elements of an ICA, including the optical recording, the information storage and the electronic, electrical transduction of the recorded input. The system, however, lacks the important feature of amplification of the recorded signal. The redox potential of the phenoxynaphthacene quinone monolayer

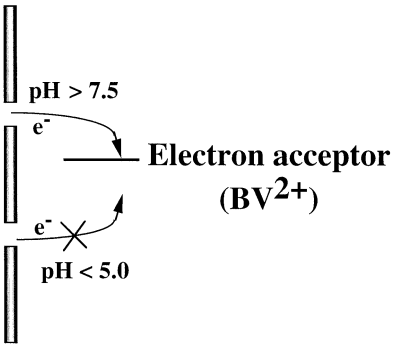

Scheme 5. Light-triggered and pH-controlled electrocatalytic processes at phenoxynaphthacene quinone–C_{14}SH mixed monolayer electrode

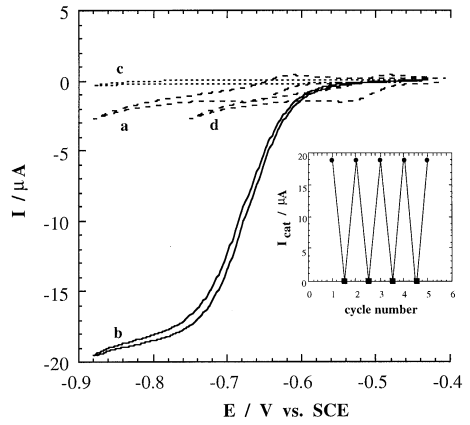

Figure 5. Cyclic voltammograms of the **2a**–or **2b**–C_{14}SH mixed monolayer Au electrode: (a) *trans*-state (**2a**) vs background solution only (pH 9.2); (b) *trans*-state (**2a**) in the presence of *N,N*′-dibenzyl-4,4′-bipyridinium salt, BV^{2+} (**3**) (1×10^{-3} M) (pH 9.2); (c) 'ana'-state (**2b**) in the presence of *N,N*′-dibenzyl-4,4′-bipyridinium salt, BV^{2+} (**3**) (1×10^{-3} M) (pH 9.2); (d) *trans*-state (**2a**) in the presence of *N,N*′-dibenzyl-4,4′-bipyridinium salt, BV^{2+} (**3**) (1×10^{-3} M) (pH 5.0). Background, 0.01 M phosphate buffer (pH 9.2 or 5.0) and 0.1 M Na_2SO_4; potential scan rate, 5 mV s^{-1}. Inset: cyclic variations of the electrocatalytic currents upon reversible photochemical transformation of the quinone from the **2a** state to the **2b** state and back. Electrocatalytic currents correspond to the current difference of the system in the presence and absence of the substrate

at pH 7.0 is $E° = -0.62$ V vs SCE. This redox potential is pH-controlled and at lower pH values the redox potential of the monolayer is shifted positively. For example, at pH 5.0 the redox potential of the quinone is shifted to $E°' = -0.51$ V vs SCE. In the presence of a redox substrate in the electrolyte solution, exhibiting a reduction potential that is more positive than the monolayer redox potential, vectorial electron transfer at the monolayer interface will proceed (Scheme 4). As the direct electrical contact of the redox probe and the electrode is blocked by the densely packed monolayer, the quinone-mediated reduction of the redox probe represents an electrocatalytic process and provides a means to amplify the electrical features of the monolayer interface.[26]

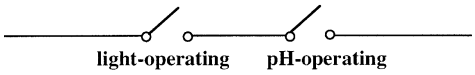

"AND"-Gate

Scheme 6. 'AND' gate electrical scheme

The amplification of the electrochemical response of the phenoxynaphthacene quinone monolayer was examined by the application of *N,N*′-dibenzyl-4,4′-bipyridinium salt, BV^{2+} (**3**), as a redox probe in the electrolyte solution, (Scheme 4). The redox potential of BV^{2+} is pH independent, $E° = -0.58$ V vs SCE. Therefore, the mediated reduction of BV^{2+} by the quinone monolayer can be controlled by the pH of the electrolyte solution as detailed in Scheme 5. At pH 7.5, the phenoxynaphthacene quinone monolayer is thermodynamically capable of electrocatalyzing the reduction of BV^{2+}, whereas acidification of the electrolyte solution to pH 5.0 generates a redox-active monolayer that is unable to catalyze the reduction of BV^{2+}. That is, the reduction of BV^{2+} by the phenoxynaphthacene monolayer electrode can be blocked by two different signal inputs: (i) photoisomerization of the monolayer to the 'ana'-quinone state and (ii) acidification of the electrolyte solution to pH 5.0. Figure 5 shows the cyclic voltammogram of the phenoxynaphthacene quinone monolayer electrode at pH 7.5 without added BV^{2+} to the electrolyte solution (curve a) and in the presence of added BV^{2+} (curve b). Addition of BV^{2+} results in an electrocatalytic

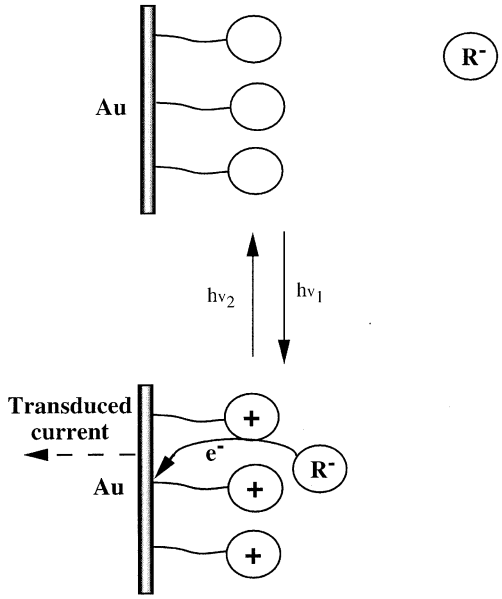

Scheme 7. Photochemically controlled electrochemical oxidation (or reduction) of positively and negatively charged electroactive probes at a photoisomerizable monolayer-modified electrode

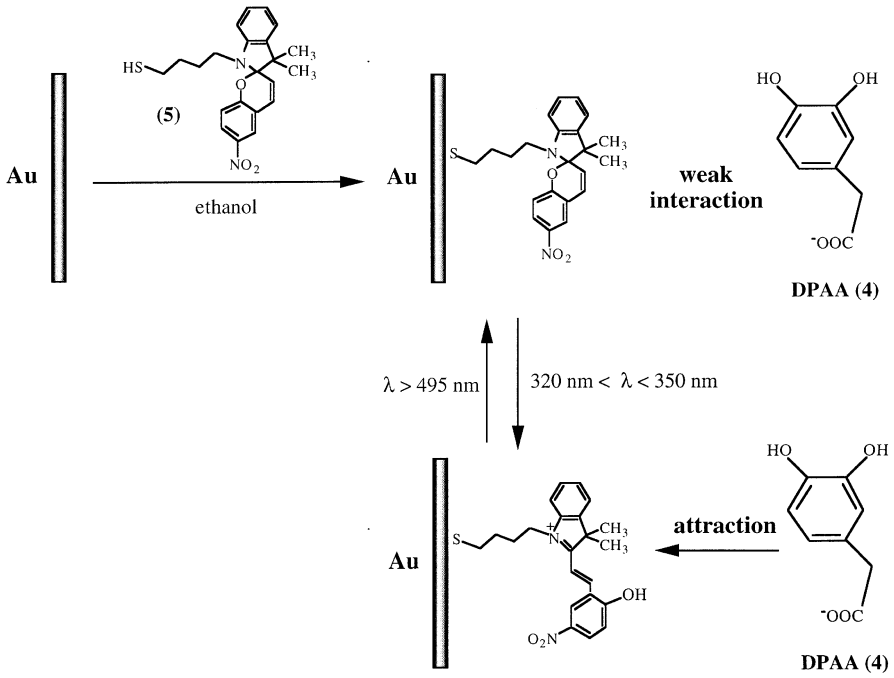

Scheme 8. Assembly and photoisomerization of a nitrospiropyran **(5)** monolayer. Charge-controlled electrochemical oxidation of DPAA **(4)** at the photoisomerizable interface

cathodic current at the redox potential characteristic of the quinone monolayer. These results clearly indicate that the quinone monolayer acts as electrocatalytic interface for the mediated, vectorial reduction of BV^{2+}. Photoisomerization of the monolayer between 305 and 320 nm to the 'ana'-quinone state with added BV^{2+} results in the electrochemical response shown in Fig. 5, curve c. No electrical response is observed, implying that the electrocatalyzed reduction of BV^{2+} is blocked and the monolayer itself is redox-inactive. Photoisomerization of the 'ana'-quinone monolayer to the phenoxynaphthacene quinone configuration above 430 nm restores the electrocatalyzed reduction of BV^{2+} to the respective radical cation, $BV^{+\cdot}$. By the cyclic photoisomerization of the monolayer between the phenoxynaphthacene quinone and 'ana'-quinone states, reversible amplified amperometric transduction of the photonic signals that activate the monolayer electrode is accomplished (Fig. 5, inset). The electrochemical response of the photoisomerizable monolayer electrode in the presence of BV^{2+} at pH 5.0 is displayed in Fig. 5, curve d. The phenoxynaphthacene quinone electrode by itself shows a positively shifted cyclic voltammogram. Addition of BV^{2+} does not yield any electrocatalyzed reduction of BV^{2+} (curve d), implying that at this pH the quinone monolayer does not mediate the reduction of BV^{2+}. Photoisomerization of the monolayer to the 'ana'-quinone state blocks the electrical response of the electrode itself.

The system for the amplified amperometric transduction of optical signals recorded by the photoisomerizable quinone monolayer electrode, and BV^{2+} acting as electron sink, mimics functions of a logic 'AND' electronic gate (Scheme 6). Such an electronic circuit is activated only upon the simultaneous input of two electronic gating signals. The similarities of the functions of the monolayer electrode to such an 'AND' electronic gate are easily visualized by initiating the photostimulated electrobiocatalyzed reduction of BV^{2+}, using the 'ana'-quinone monolayer electrode at pH 5.0. Application of a potential corresponding to $E^\circ = -0.62$ V vs SCE to the electrode does not yield the reduction of BV^{2+}, and no electrocatalytic cathodic current is observed. Light-induced isomerization of the monolayer to the naphthacene quinone state does not stimulate the electrocatalyzed reduction of BV^{2+} since the pH of the medium is acidic. Photoisomerization to the quinone state and adjustment of the pH to 7.5 switch on the two gates and electrocatalyzed reduction of BV^{2+} proceeds. Opening any of these gates blocks the reduction of BV^{2+} and the transduced amperometric signal.

A NITROSPIROPYRAN MONOLAYER-FUNCTIONALIZED ELECTRODE: A COMMAND SURFACE FOR CONTROLLING INTERFACIAL ELECTRON TRANSFER

A different approach to transduce electrochemically photonic signals recorded by a photosensitive monolayer-functionalized electrode involves the application of a photoisomerizable monolayer electrode as a command surface for the controlled interfacial electron transfer

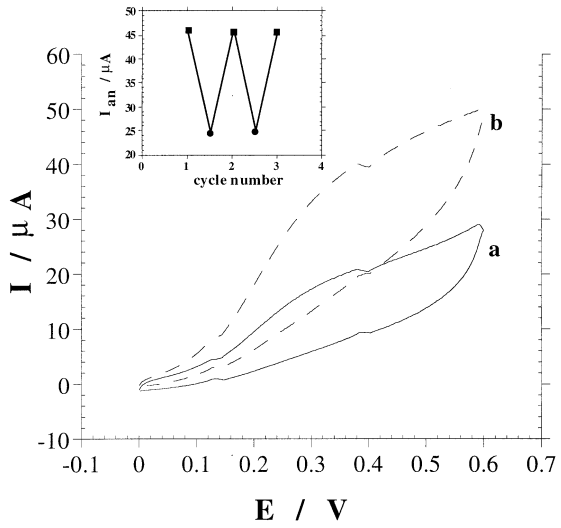

Figure 6. Cyclic voltammograms at the photoisomerizable **5** monolayer-modified Au electrode in the presence of 5×10^{-4} M DPAA: (a) in the presence of SP-state monolayer produced by illumination (>495 nm) and (b) in the presence of MRH^+ state monolayer produced by irradiation (320–350 nm). Background electrolyte, 0.02 M phosphate buffer (pH 7.0); potential scan rate, 200 mV s^{-1}. Inset: reversible transduction of anodic currents by the photoisomerizable monolayer electrode, extracted from cyclic voltammograms of DPAA at $E = 470$ mV vs SCE: (●) SP state; (■) MRH^+ state

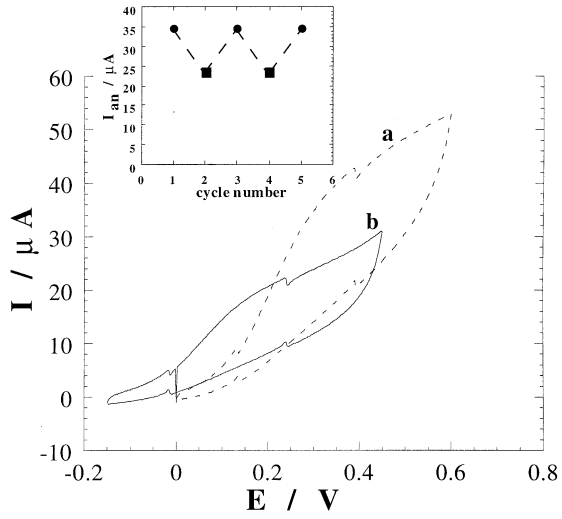

Figure 7. Cyclic voltammograms at the **5** monolayer-modified Au electrode after its irradiation (320–350 nm) in the presence of 5×10^{-4} M DPAA: (a) pH 7.0; (b) pH 9.2. Background electrolyte, 0.02 M phosphate buffer (pH 7.0 or 9.2); potential scan rate, 200 mV s^{-1}. Inset: reversible transduction of anodic currents as a function of pH, elucidated from cyclic voltammograms of DPAA at $E = 300$ mV vs SCE: (●) pH 7.0; (■) pH 9.2

(Scheme 7). The photoisomerizable monolayer associated with the electrode undergoes light-induced isomerization between a neutral and a positively charged state. A negatively charged redox probe, R^-, is used to transduce electrically the photochemical reaction occurring at the monolayer interface. In the neutral state, no electrical interaction between the electrode and the redox probe exists. The electrical response is diffusion controlled and eventually associated with kinetic barriers. Photoisomerization to the positively charged photoisomer monolayer state results in the electrostatic attraction of the redox probe. The concentration of the redox probe at the electrode surface improves its electrical contact, and a high amperometric response of the electrode is expected.

This approach was materialized by the organization of a nitrospiropyran photoisomerizable monolayer on an Au electrode and the application of the interface as a photosensitive command surface for the controlled interfacial oxidation of dihydroxyphenylacetic acid (DPAA) (**4**)[27] to the respective *o*-quinone. The photoisomerizable monolayer was organized by the immobilization of mercaptobutylnitrospiropyran (**5**) on an Au electrode (Scheme 8). The monolayer-functionalized electrode exhibits reversible photoisomerization and UV irradiation of the neutral nitrospiropyran monolayer state between 320 and 350 nm, yields, in aqueous solution (pH 7.0), the protonated nitromerocyanine, positively charged, monolayer, whereas illumination of the latter interface with visible light above 495 nm regenerates the nitrospiropyran monolayer state. Electrostatic attraction of DPAA (**4**) to the positively charged, protonated nitromerocyanine is expected to enhance the electrooxidation of the substrate owing to its concentration at the electrode surface. Figure 6 shows the light-stimulated electrical responses of DPAA in the presence of the photoisomerizable monolayer electrode. With the neutral nitrospiropyran monolayer, a weak amperometric response is observed (curve a) whereas photoisomerization of the monolayer to the protonated nitromerocyanine yields an enhanced amperometric response (curve b). The accelerated, irreversible oxidation of DPAA at the positively charged monolayer interface is attributed to the electrostatic attraction of the electroactive substrate by the functionalized electrode, leading to a high local concentration of the redox substrate at the interface. By cyclic photoisomerization of the monolayer between the neutral and positively charged states, the amperometric responses of the electrode are switched between high ('On') and low ('Off') values (see inset, Fig. 6). Hence, the photonic information recorded by the monolayer generates an active interface for controlling the electrochemical processes of charged redox species at the electrode interface. Oxidation of DPAA by the protonated nitromerocyanine monolayer electrode provides a means for the amperometric transduction of the optical signal that activates the respective isomer state of the monolayer.

The protonation of the nitromerocyanine monolayer interface is controlled by the pH of the electrolyte

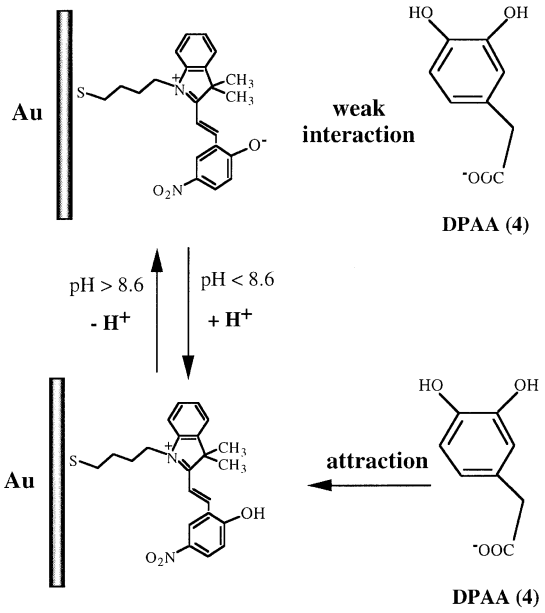

Scheme 9. pH-controlled electrochemical oxidation of DPAA **(4)** at a nitrospiropyran, **(5)** monolayer photoisomerizable electrode

solution. At pH > 8.6, the nitromerocyanine exists in a neutral, zwitterionic, state and thus the electrostatic attraction of DPAA to the electrode surface is perturbed. Figure 7 shows the cyclic voltammograms of DPAA (**4**) in the presence of the nitromerocyanine at pH 7.0 and 9.2 (curves a and b, respectively). Note that the amperometric response of the nitromerocyanine monolayer at pH 9.2 is low and shifted to more negative potentials compared with the electrical response of DPAA with the nitromerocyanine monolayer at pH 7.0. The amperometric response of the nitromerocyanine monolayer-electrode at pH 9.2 is almost identical to the amperometric response of DPAA in the presence of the nitrospiropyran monolayer-electrode at pH 7.0 (compare curve a, Fig. 6 and curve b, Fig. 7). These results imply that the nitromerocyanine exists at pH 9.2 as a zwitterionic, betaine monolayer that does not attract the redox probe to the electrode surface. The negative shift of the oxidation current of DPAA on changing the pH to 9.2 is consistent with the fact that electrooxidation of **4** is pH dependent, and its oxidation potential is negatively shifted in basic aqueous environments. The feasibility of controlling the electrical features of the monolayer associated with the electrode by two physical inputs, i.e. photonic and pH signals, allows us to design with this photoisomerizable monolayer a gated 'AND' optoelectronic system. The system rests in the nitrospiropyran monolayer state, pH 9.2. In the presence of DPAA, a low amperometric response is observed, as the redox probe does not interact with the monolayer. Photoisomerization of the monolayer to the nitromerocyanine state does not alter the magnitude of the electrical response, since the monolayer exists in a zwitterionic state. Acidification of the electrolyte solution to the protonated monolayer state

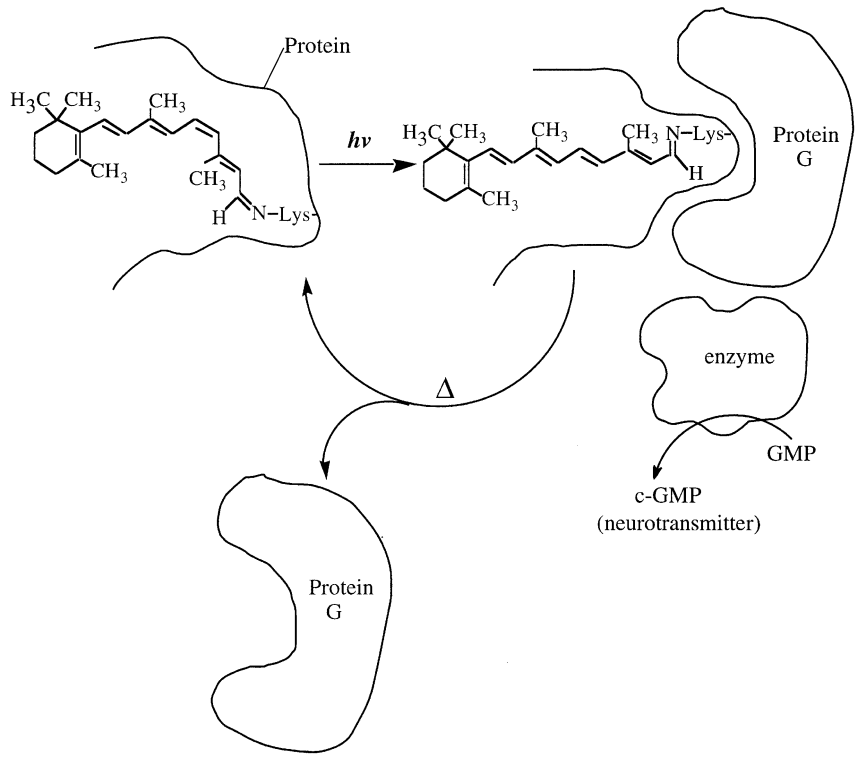

Scheme 10. Schematic functions of the vision process

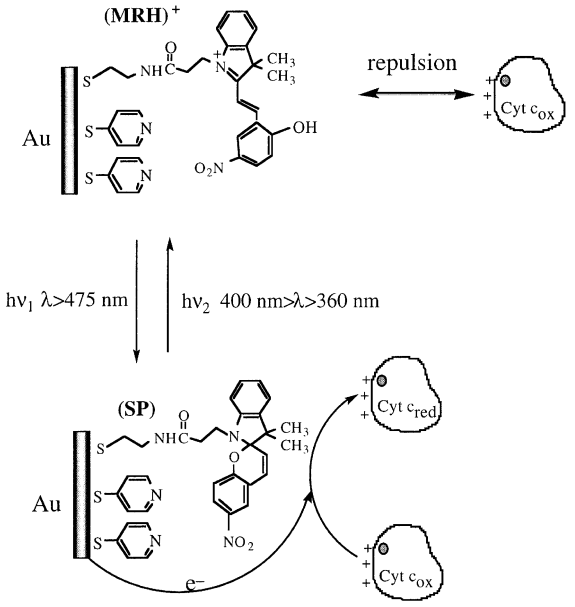

Scheme 11. Photochemically controlled electron transfer communication of Cyt *c* with the nitrospiropyran **(5)** photoisomerizable monolayer electrode

results in the effective electrooxidation of DPAA and a high current transduction. Alternatively, the high amperometric response can be achieved by adjusting the electrolyte solution to pH 7.0 followed by photoisomerization of the nitrospiropyran monolayer to the nitromerocyanine monolayer state. That is, the nitrospiropyran monolayer electrode at pH 7.0 is activated for the electrochemical oxidation of DPAA only upon application of the two complementary signals: (i) transformation of the pH from 9.2 to 7.0 (Scheme 9) and (ii) photoisomerization of the nitrospiropyran monolayer state to the nitromerocyanine configuration (Scheme 8).

A PYRIDINE–NITROSPIROPYRAN MIXED MONOLAYER ELECTRODE: A COMMAND INTERFACE FOR PHOTONIC CONTROL OF THE ELECTRICAL CONTACT OF CYTOCHROME *c* WITH THE ELECTRODE

The vision process represents a biological optoelectronic system where light signals translate into neural responses. Scheme 10 shows schematically the features of the natural process. The 11-*cis* retinal chromophore embedded in the protein, undergoes light-induced isomerization to the all-*trans*-chromophore. The structural photoisomerization of the chromophore stimulates a configurational change in the surrounding protein, that leads to the formation of a binding site for protein G. Association of protein G with the protein activates an enzyme cascade that generates the neurotransmitter c-GMP, which in turn activates the neural response. Relaxation of the chromophore to the 11-*cis* state dissociates protein G and the enzyme cascade that yields c-GMP is blocked. This evolutionary developed biological optoelectronic system includes several elements that need to be addressed in order to develop future optobioelectronic mimetic systems. (i) The chromophore stimulates a structural change in the surrounding protein. This is accompanied by the formation of a binding site for protein G. That is, the protein structure is triggered by the photoisomerizable chromophore to yield a command interface for the binding and dissociation of protein G. (ii) Activation of the enzyme cascade by protein G provides a means for the biocatalytic amplification of the binding interactions between protein G and the protein association site. (iii) The system relaxes rapidly to its original state, thereby restoring the optical sensor assembly.

We have designed an artificial approach to tailor systems that mimic functions of the native vision process. One of these systems is based on the hemoprotein cytochrome *c* (Cyt *c*), which participates in a variety of mediated electron transfer processes in biological systems.[28] The Fe(II)/Fe(III)-protoporphyrin IX redox center is embedded in a low molecular weight protein assembly (MW, ≈12 300), and is electrically insulated for direct electrical communication with electrode surfaces. Application of special conductive supports, e.g. glassy carbon[29] or an In_2O_3 electrode,[30] or surface modification of electrodes with promoter units[31–33] such as pyridine,[34,35] thiophene[36] or imidazole[37] were reported to enhance the electrical contact between Cyt *c* and the electrode. It was suggested that association of Cyt *c* to the promoter substrate aligns the protein redox center relative to the electrode, so that short electrode transfer distances are attained. For example, Cyt *c* was found[38] to bind to a thiolpyridine monolayer associated with an Au electrode,

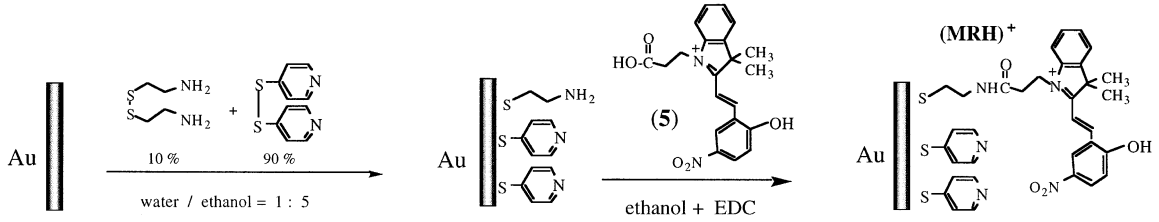

Scheme 12. Organization of photoisomerizable nitrospiropyran–pyridine mixed monolayer electrode

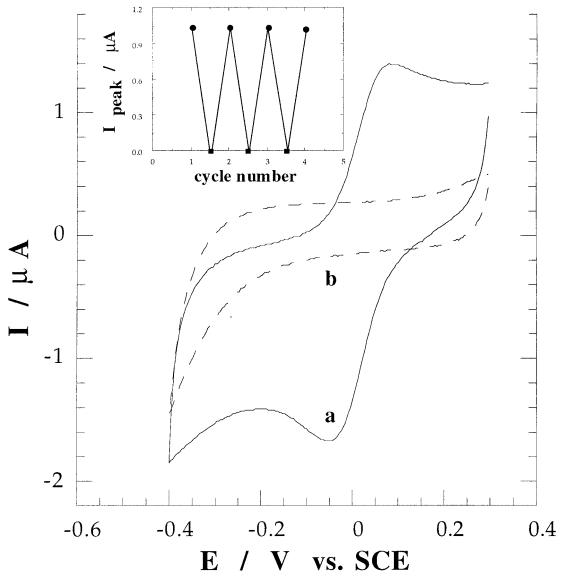

Figure 8. Cyclic voltammograms of Cyt *c* (1×10^{-4} M) recorded at a potential scan rate of 50 mV s^{-1} in 0.1 M Na_2SO_4 and 0.01 M phosphate buffer (pH 7.0): (a) in the presence of the SP–pyridine mixed monolayer electrode; (b) in the presence of the MRH^+–pyridine mixed monolayer electrode. Inset: cyclic amperometric responses of Cyt *c* in the presence of the different photoisomer states of the monolayer electrode

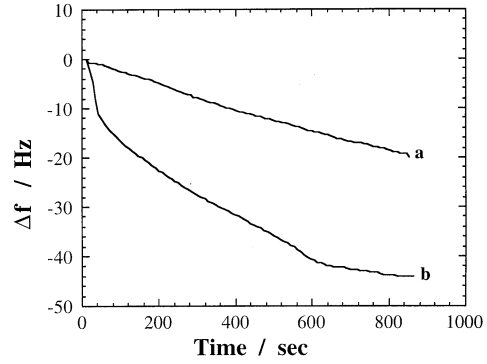

Figure 9. Time-dependent frequency changes of a pyridine–nitrospiropyran-functionalized Au quartz crystal (9 MHz) upon interaction with Cyt *c:* (a) 1×10^{-8} M; (b) 1×10^{-5} M. Measurements performed in 0.1 M phosphate buffer (pH 7.0)

$K_a = 8.5 \times 10^{-3}\ M^{-1}$. The affinity interactions existing between Cyt *c* and a pyridine monolayer, and the fact that Cyt *c* is a positively charged protein at neutral pH, p*I* = 10.0, were used to organize an optobioelectronic assembly (Scheme 11). A mixed monolayer consisting of thiolpyridine and nitrospiropyran units was assembled on an Au electrode. Association of Cyt *c* with the pyridine binding sites yields electrical communication between the hemoprotein and the electrode. Photoisomerization of the monolayer to the pyridine-protonated merocyanine mixed monolayer state generates a positively charged interface. This perturbs the association of Cyt *c* to the monolayer owing to electrostatic repulsion of the protein

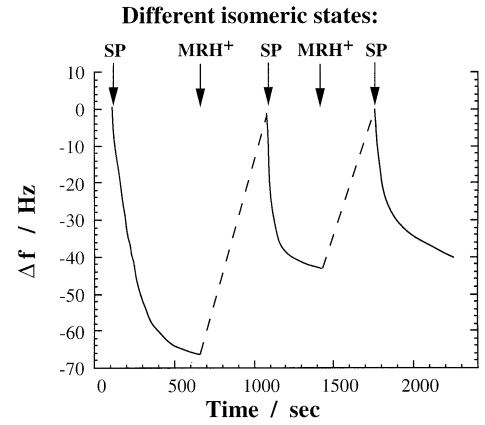

Figure 10. Cyclic frequency changes of the nitrospiropyran–pyridine photoisomerizable mixed monolayer functionalized Au quartz crystal in the presence of Cyt *c* (1×10^{-4} M) upon reversible photoisomerization of the electrode between the nitrospiropyran (SP) and protonated merocyanine (MRH^+) monolayer states. Measurements performed in 0.1 M phosphate buffer (pH 7.0)

from the pyridine sites. Scheme 12 shows the synthetic method for assembling the thiolpyridine–nitrospiropyran monolayer electrode. The primary step involved the assembly of the thiolated pyridine and cystamine mixed monolayer followed by covalent coupling of *N*-carboxyethylnitrospiropyran **(5)** to the monolayer.

Figure 8 shows the cyclic voltammograms upon photoisomerization of the mixed monolayer electrode in the presence of Cyt *c*. In the presence of the pyridine–nitrospiropyran, a quasi-reversible redox wave of Cyt *c* at $E^\circ = +0.01$ V vs SCE is observed (curve a). This electrical response is attributed to effective electrical communication between the heme site and the electrode, owing to the affinity binding of Cyt *c* to the pyridine sites. Photoisomerization of the monolayer to the pyridine–protonated nitromerocyanine blocks the electrical contact between Cyt *c* and the electrode (curve b). This originates from the electrostatic repulsion of Cyt *c* from the positively charged monolayer interface. Cyclic photoisomerization of the monolayer electrode between the nitrospiropyran and protonated nitromerocyanine states results in photoswitchable electrical contact between the hemoprotein and the electrode (Fig. 8, inset). Hence the photostimulated structural isomerization of the monolayer induces the binding and dissociation of Cyt *c* to and from the interface, processes that are being transduced by the amperometric responses of the modified electrode. The light-controlled association and dissociation of Cyt *c* to and from the photoisomerizable monolayer mimic the affinity interaction functions existing between protein G and the retinal protein in the vision process.

Further support for the binding of Cyt *c* to the pyridine–nitrospiropyran monolayer and photostimulated association and dissociation of the hemoprotein to and from the monolayer is obtained from microgravimetric

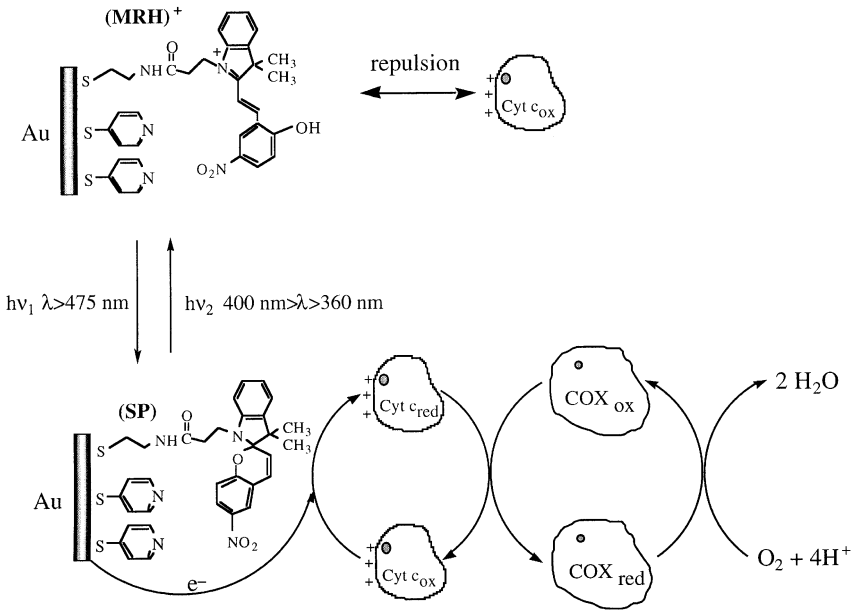

Scheme 13. Coupling of photochemically controlled electrical interactions of Cyt *c* with the nitrospiropyran photoisomerizable monolayer to the biocatalyzed reduction of O_2 by cytochrome oxidase (COx)

quartz crystal microbalance measurements.[38] The resonance frequency of piezoelectric quartz crystals is controlled by, among various other parameters, the crystal thickness (or its mass). A mass change occurring on the quartz crystal induces a frequency change, Δf, expressed by the Sauerbrey equation:[39]

$$\Delta f = -\left(\frac{f_0^2}{N\rho_q}\right)\Delta m = -C_f \Delta m \qquad (1)$$

where f_0 is the basic frequency of the crystal, ρ_q is the density of quartz and N is the frequency constant of the crystal. For quartz crystals of basic frequency corresponding to 9 MHz, the value of C_f is 1.83×10^8 Hz g^{-1} cm^2. Hence an increase in the crystal mass, i.e. by association of Cyt *c* with the crystal, is expected to yield a decrease in the crystal frequency, whereas a decrease in the crystal mass, resulting from the dissociation of Cyt *c*, should yield an increase in the crystal frequency.

Quartz crystals (*ca* 9 MHz) that include two Au electrodes were used as the interface for the microgravimetric analysis of the interactions of Cyt *c* with the photoisomerizable monolayer. The Au electrodes were modified with a pyridine–nitrospiropyran monolayer, as outlined in Scheme 12. Figure 9 shows the crystal frequency changes on interaction with different concentrations of Cyt *c* in the bulk solution. The decrease in the crystal frequency implies an increase in the crystal mass as a result of the association of Cyt *c* with the pyridine units of the monolayer assembly. The time-dependent frequency changes of the crystal upon interaction with Cyt *c*, represent the kinetics of association of Cyt *c* with the monolayer. The change in the crystal frequency increases as the bulk concentration of Cyt *c* is elevated. The frequency change observed at a bulk concentration of Cyt *c* corresponding to 1×10^{-5} M (Fig. 9, curve b) represents the saturation of the monolayer by the hemoprotein. From the total frequency change of the crystal, and using Eqn (1), we calculate the surface coverage of Cyt *c* on the Au electrode to be 9×10^{-12} mol cm^{-2}. This experimental surface coverage of the Au support by Cyt *c* is in agreement with the theoretical value of a randomly densely packed Cyt *c* layer. The diameter of the Cyt *c* molecule is 0.38×10^{-6} cm, which translates to an area projection of 1.13×10^{-13} cm^2, and a surface coverage of a densely packed monolayer that corresponds to 1.47×10^{-11} mol cm^{-2}. A randomly densely packed protein monolayer of a protein was estimated to reveal *ca* 60% of the surface coverage of an organized, aligned protein layer. Hence the calculated coverage of the randomly densely packed monolayer by Cyt *c* is 9×10^{-12}, a value that is in agreement with the experimental surface density. Control experiments revealed that no frequency change of the crystal occurs upon interaction of the pyridine–protonated merocyanine monolayer-functionalized crystal with Cyt *c*. These results imply that Cyt *c* is not associated with this photoisomer-state of the monolayer.

The cyclic association and dissociation of Cyt *c* to and from the pyridine-photoisomerizable monolayer can be followed by microgravimetric, quartz crystal microbalance transduction (Fig. 10). Interaction of the pyridine–nitrospiropyran monolayer-functionalized crystal with Cyt *c* yields a decrease in the crystal frequency. Photoisomerization of the monolayer to the protonated nitromerocyanine followed by rinsing of the crystal results in the original base frequency of the crystal that is not affected by the addition of Cyt *c*. Photoisomerization of the monolayer to the nitrospiropyran state is

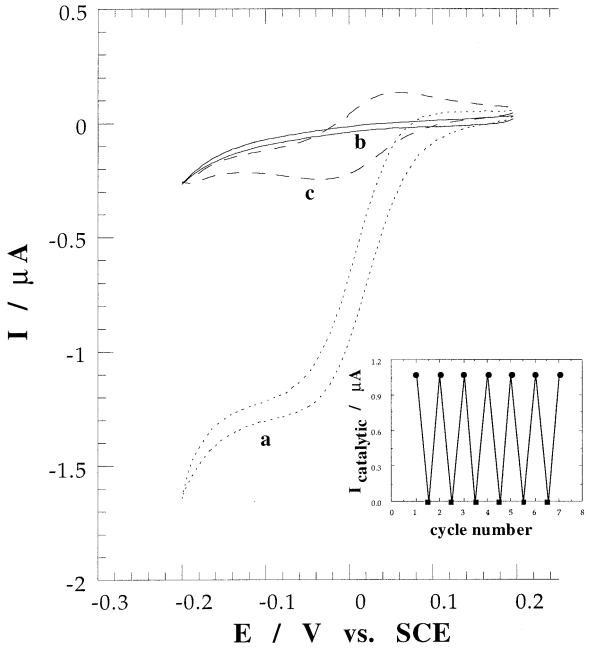

Figure 11. Cyclic voltammograms of Cyt *c* (1×10^{-4} M) and cytochrome oxidase (COx), (1×10^{-6} M), recorded at a potential scan rate of 2 mV s^{-1} in 0.1 M Na_2SO_4 and 0.1 M phosphate buffer (pH 7.0): (a) in the presence of O_2 (air) and the SP–pyridine mixed monolayer electrode; (b) in the presence of O_2 (air) and the MRH^+–pyridine mixed monolayer electrode; (c) in the absence of COx and in the presence of O_2 (air) with the SP–pyridine monolayer electrode. Inset: cyclic amperometric responses of the photoisomerizable monolayer electrode in the presence of Cyt *c*–COx–O_2

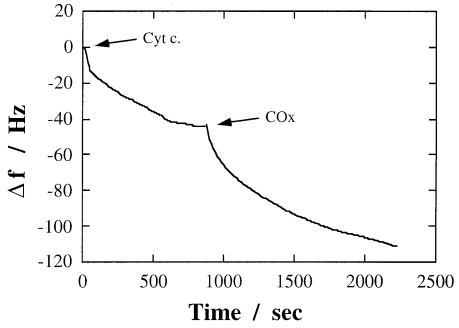

Figure 12. Time-dependent frequency changes of the nitrospiropyran–pyridine mixed monolayer Au quartz crystal (AT-cut, 9 MHz) upon interaction with Cyt *c* (1×10^{-5} M) and COx (1×10^{-7} M). Arrows indicate the time of introduction of Cyt *c* and COx, respectively. Measurements were performed in 0.1 M phosphate buffer (pH 7.0). Cell solution that included Cyt *c* was replaced and the electrode was washed with the phosphate buffer prior to the introduction of COx

accompanied by a frequency decrease that indicates the binding of the hemoprotein to the crystal interface. By cyclic photoisomerization of the monolayer between the two states, the association of Cyt *c* with the pyridine–nitrospiropyran monolayer and the dissociation of Cyt *c* from the pyridine–protonated nitromerocyanine, is reversibly sensed by the piezoelectric signal. It should be noted that photoisomerization of the monolayer interface to the pyridine–nitrospiropyran state does not yield similar frequency changes, Δf, in the different irradiation cycles. This is attributed to experimental difficulties associated with the precise re-positioning of the crystal in the cell after each illumination cycle that is performed outside the cell.

AMPLIFIED AMPEROMETRIC TRANSDUCTION OF OPTICAL SIGNALS RECORDED BY A PYRIDINE–NITROSPIROPYRAN MONOLAYER ELECTRODE IN THE PRESENCE OF CYTOCHROME *c*–CYTOCHROME OXIDASE

Photostimulated association and dissociation of Cyt *c* to the pyridine–nitrospiropyran mixed monolayer mimic the primary interactions of protein G with rhodopsin. The photoswitchable electrical contact of Cyt *c* with the electrode transduces the photonic signal recorded by the monolayer, yet the transduced signal is not an amplified output. To design the amplification element, a catalytic chemical event that turns over the electrical contact of Cyt *c* with the electrode is needed. As Cyt *c* acts as electron mediator in a variety of enzyme-catalyzed redox transformations,[40,41] such an amplification route seems feasible. This will be described here with the photoswitchable, Cyt *c*-mediated, electrobiocatalyzed reduction of molecular oxygen using cytochrome oxidase, COx. The pyridine–nitrospiropyran monolayer electrode shown in Scheme 9 was used as the command interface that controls the electrical contact with Cyt *c*. The hemoprotein was used as electron mediator that controls the COx-biocatalyzed reduction of O_2 (Schene 13). Figure 11 shows the cyclic voltammograms of the pyridine–nitrospiropyran monolayer electrode in the presence of Cyt *c*–COx–O_2 (curve a). Control experiments revealed that no electrocatalytic cathodic current is obtained in the absence of Cyt *c*, COx or oxygen. Hence the high electrocatalytic cathodic current implies the effective Cyt *c*-mediated reduction of O_2 by COx. Photoisomerization of the monolayer to the pyridine–protonated nitromerocyanine state results in the cyclic voltammogram shown in Fig. 11, curve (b). The electrical response is completely blocked, implying that perturbation of the electrical contact between Cyt *c* and the electrode eliminates the COx-biocatalyzed reduction of O_2. Figure 11, compares the electrical response of Cyt *c* alone in the presence of the pyridine–nitrospiropyran monolayer electrode (curve c) to the amperometric output observed in this system upon addition of COx–O_2, (curve a). Clearly, addition of the COx biocatalyst and oxygen amplifies the amperometric response of the functiona-

lized electrode. The pyridine–nitrospiropyran monolayer electrode facilitates the electrical contact between Cyt *c* and the electrode by association of Cyt *c* with the pyridine sites. Cyt *c*-mediated electron transfer to COx induces the biocatalyzed reduction of O_2. The electron transfer from the hemoprotein to COx regenerates oxidized Cyt *c*. As the electrode-associated oxidized Cyt *c* is further reduced, the electron transfer to a single Cyt *c* layer is turned over by the biocatalyzed reduction of O_2. This yields an amplified amperometric response of the electrode (Scheme 13). Photoisomerization of the monolayer to the pyridine–protonated merocyanine state results in the dissociation of Cyt *c* from the monolayer interface. This blocks the electrical contact between Cyt *c* and the electrode and inhibits the COx-biocatalyzed reduction of O_2 (Scheme 13). By reversible photoisomerization of the monolayer between the pyridine–nitrospiropyran and pyridine–protonated nitromerocyanine states, cyclic amplified amperometric transduction of the optical signals recorded by the monolayer is achieved (inset, Fig. 11). The photostimulated, Cyt *c*-mediated, COx-bioelectrocatalyzed reduction of oxygen in the presence of the photoisomerizable monolayer mimics the basic elements of the vision process. The photoinduced association and dissociation of Cyt *c* to and from the monolayer duplicates binding and displacement of protein G to and from the protein of the vision system. The Cyt *c*-mediated electron transfer to COx, and the activation of the biocatalyzed reduction of O_2 in the presence of the pyridine–nitrospiropyran monolayer, mimic the functions of protein G-activated enzyme cascade in the vision process.

A further aspect that should be addressed relates to the protein–protein interactions between Cyt *c* and COx that lead to the mediated electron transfer and the reduction of O_2. Microgravimetric, quartz crystal microbalance experiments revealed the formation of a Cyt *c*–COx complex at the photoisomerizable monolayer. The pyridine–nitrospiropyran mixed monolayer was assembled on Au electrodes associated with a piezoelectric quartz crystal (9 MHz). The electrode was interacted with Cyt *c* (1×10^{-4} M) and a decrease of $\Delta f \approx -40$ Hz in the crystal frequency was observed (Fig. 12). The Cyt *c*-functionalized monolayer was then interacted with 1×10^{-7} M COx, which yielded a further decrease in the crystal frequency of $\Delta f \approx -75$ Hz (Fig. 12). Using Eqn (1) and the molecular weight of COx (*ca* 200 000), the surface coverage of the monolayer by COx corresponds to *ca* 5.8×10^{-13} mol cm^{-2}. Control experiments revealed that neither Cyt *c* nor COx induced any frequency change of the crystal in the pyridine–protonated merocyanine state. Also, photoisomerization of the pyridine–nitrospiropyran monolayer assembled on the crystal with the Cyt *c*–COx complex to the pyridine–nitromerocyanine state results in the restoration of the initial crystal frequency, indicating that the protein–protein complex was dissociated from the monolayer interface. These results clearly indicate that a complex between COx and Cyt *c* is formed on the base monolayer of pyridine–nitrospiropyran. This complex presumably leads to short distances between the heme center of Cyt *c* and the redox sites of COx. The electrical contact of the heme site and the electrode facilitates the electron transfer to COx within the complex assembly.

CONCLUSIONS AND PERSPECTIVES

This paper has addressed the chemical architecture of two-dimensional photoisomerizable monolayers on conductive supports. The photoisomerizable monolayers were applied as light-triggered 'command surfaces' for controlling redox processes of molecular and biomolecular substrates at the monolayer interface. The photoswitchable redox processes at the functionalized electrodes led to the amperometric transduction of optical signals recorded by the monolayer. Coupling of the light-triggered redox reactions with secondary electrocatalyzed chemical transformations provides a general means for the *amplified* amperometric transduction of the photonic signals.

Dual activation of functionalized monolayers by two different physicochemical signals allows the design of gated molecular and biomolecular electronic systems. The present account has addressed the use of photonic and pH input signals that control the redox features and/or the electrical properties of the monolayers. With these systems, gated 'AND' molecular logic gates were tailored. Other molecular gates such as 'OR', 'OR' and 'AND' could be designed by analogous approaches.

The molecular and biomolecular optoelectronic systems described here are nano-structured two-dimensional molecular arrays. The systems are triggered by optical signals and transduce electrically the recorded input. Significant advances have been accomplished in recent years in the micro-patterning of surfaces with monolayer assemblies. Also, nanoscale irradiation of microscopic domains was achieved by the application of near-field scanning optical microscopy (NSOM), and imaging of the optically treated domains is feasible by various scanning probe microscopic techniques (AFM, STM, etc.). It is a future challenging scientific effort to apply these techniques to manipulate photosensitive monolayer arrays for dense storage of photonic information and nanoscale wiring of molecular electronic gates.

Acknowledgment

This research was supported by the Israel Science Foundation.

REFERENCES

1. F. L. Carter, R. E. Siatkowsky and H. Woltjien (Eds). *Molecular Electronic Devices.* Elsevier, Amsterdam (1988).
2. J. M. Lehn. *Angew. Chem., Int. Ed. Engl.* **27,** 90 (1988).
3. J. M. Lehn (Ed.). *Supramolecular Chemistry.* VCH, Weinheim (1995).
4. M. R. Wasielewski, M. P. O'Neil, D. Gosztola, M. P. Niemczyk and W. A. Svec. *Pure Appl. Chem.* **64,** 1319 (1995).
5. P. Ball and L. Garwin. *Nature (London)* **355,** 761 (1992).
6. L. Fabbrizzi and A. Poggi. *Chem. Soc. Rev.* **24,** 197 (1995).
7. K. E. Drexel (Ed.). *Nanosystems: Molecular Machinery, Manufacturing and Computation.* Wiley, New York (1992).
8. L. F. Lindoy. *Nature (London)* **364,** 17 (1993).
9. C. A. Mirkin and M. A. Ratner. *Annu. Rev. Phys. Chem.* **43,** 719 (1992).
10. N. P. M. Huck and B. L. Ferringa. *J. Chem. Soc., Chem. Commun.* 1095 (1995).
11. S. H. Kawai, S. L. Gilat and J. M. Lehn. *J. Chem. Soc., Chem. Commun.* 1011 (1994).
12. S. L. Gilat, S. H. Kawai and J. M. Lehn. *Chem. Eur. J.* **1,** 275 (1995).
13. S. H. Kawai, S. L. Gilat, R. Ponsinet and J. M. Lehn. *Chem. Eur. J.* **1,** 285 (1995).
14. J. Daub, C. Fischer, J. Salbeck and K. Ulrich. *Adv. Mater.* **3,** 366 (1990).
15. K. Morigaki, Z. Liu, K. Hashimoto and A. Fujishima. *J. Phys. Chem.* **99,** 14771 (1995).
16. Z. Liu, K. Hashimoto and A. Fujishima. *Nature (London)* **347,** 658 (1990).
17. K. T. Ranjit, S. Marx-Tibbon, I. Ben-Dov, B. Willner and I. Willner. *Isr. J. Chem.* **36,** 407 (1996).
18. S. Marx-Tibbon, I. Ben-Dov and I. Willner. *J. Am. Chem. Soc.* **118,** 4717 (1996).
19. M. Lahav, K. T. Ranjit, E. Katz and I. Willner. *Chem. Commun.* 259 (1997).
20. I. Willner and S. Rubin. *Angew. Chem., Int. Ed. Engl.* **35,** 367 (1996).
21. M. Lion-Dagan, E. Katz and I. Willner. *J. Am. Chem. Soc.* **116,** 7913 (1994).
22. I. Willner, R. Blonder, E. Katz, A. Stocker and A. F. Bückmann. *J. Am. Chem. Soc.* **118,** 5310 (1996).
23. I. Willner, A. Doron, E. Katz, S. Levi and A. J. Frank. *Langmuir* **12,** 946 (1996).
24. M. Lion-Dagan, S. Marx-Tibbon, E. Katz and I. Willner. *Angew. Chem., Int. Ed. Engl.* **34,** 1604 (1995).
25. A. Doron, E. Katz, M. Portnoy and I. Willner. *Angew. Chem., Int. Ed. Engl.* **35,** 1535 (1996).
26. A. Doron, M. Portnoy, M. Lion-Dagan, E. Katz and I. Willner. *J. Am. Chem. Soc.* **118,** 8937 (1996).
27. A. Doron, E. Katz, G. Tao and I. Willner. *Langmuir* **13,** 1783 (1997).
28. M. Lion-Dagan, E. Katz and I. Willner. *J. Chem. Soc., Chem. Commun.* 2741 (1994).
29. S. Dong and Q. Chi. *Bioelectrochem. Bioenerg.* **29,** 237 (1992).
30. I. Taniguchi, H. Kurihara, K. Yoshida, M. Tominaga and F. M. Hawkridge. *Denki Kagaku* **60,** 1043 (1992).
31. F. A. Armstrong, H. A. O. Hill and N. J. Walton. *Q. Rev. Biophys.* **18,** 261 (1986).
32. F. A. Armstrong, H. A. O. Hill and N. J. Walton. *Acc. Chem. Res.* **21,** 407 (1988).
33. J. E. Frew and H. A. O. Hill. *Eur. J. Biochem.* **172,** 261 (1988).
34. P. M. Allen, H. A. O. Hill and N. J. Walton. *J. Electroanal. Chem.* **178,** 69 (1984).
35. I. Taniguchi, K. Toyosawa, H. Yamaguchi and K. Yasukouchi. *J. Chem. Soc., Chem. Commun.* 1032 (1982).
36. X. Qu, T. Lu, S. Dong, C. Zhou and T. M. Cotton. *Bioelectrochem. Bioenerg.* **34,** 153 (1994).
37. G. Li, H. Chen and D. Zhu. *Anal. Chim. Acta*, **319,** 275 (1996).
38. M. Lion-Dagan, I. Ben-Dov and I. Willner. *Colloids Surf., B: Biointerfaces*, **8,** 251 (1997).
39. D. A. Buttry. in *Electroanalytcal Chemistry*, edited by A. J. Bard, Vol. 17, p. Marcel Dekker, New York (1991).
40. H. A. O. Hill, N. J. Walton and I. J. Higgins. *FEBS Lett.* **126,** 282 (1981).
41. A. E. G. Cass, G. Davis, H. A. O. Hill and D. J. Nancarrow. *Biochim. Biophys. Acta* **828,** 51 (1985).

